THE AMERICAN SOCIETY OF MECHANICAL ENGINEERS
345 E. 47th St., New York, N.Y. 10017

94-GT-53

ACTIVE VIBRATION CONTROL OF ROTATING MACHINERY WITH A HYBRID PIEZO-HYDRAULIC ACTUATOR SYSTEM

Punan Tang and Alan B. Palazzolo
Texas A&M University
College Station, Texas

Albert F. Kascak and Gerald T. Montague
NASA Lewis Research Center
Cleveland, Ohio

ABSTRACT

An integrated, compact piezo-hydraulic actuator system for active vibration was designed and developed with a primary application for gas turbine aircraft engines. Copper tube was chosen as the transmission line material for ease of assembly. Liquid plastic which meets incompressibility and low viscosity requirements was adjusted to provide optimal actuator performance. Variants of the liquid plastic have been prepared with desired properties between -40^0 F and 400^0 F. The effectiveness of this hybrid actuator for active vibration control (AVC) was demonstrated for suppressing critical speed vibration through two critical speeds for various levels of intentionally placed imbalance. A high accuracy closed loop simulation which combines both finite element and state space methods was applied for the closed loop unbalance response simulation with/without AVC. Good correlation between the simulation and test results was achieved.

NOMENCLATURE

C_{active}	active damping of feedback control system.
G_C	adjustable derivative path gain of hybrid controller.
G_K	adjustable proportional path gain of hybrid controller.
$G_d(s)$	unit derivative path transfer function of hybrid controller.
$G_p(s)$	unit proportional path transfer function of hybrid controller.
$G_i(s)$	feedback electromechanical component transfer function representations (i=1,...,7).
$G_{basic}(s)$	basic transfer function of digital programmable low pass filter.
G	control force distribution matrix.
$G_{HC}(s)$	hybrid controller transfer function.
$F_{out}(s)$	piezohydraulic actuator control force to rotorbearing system.
f_c	adjustable cut-off frequency of digital programmable low pass filter.
f_{co}	cut-off frequency of basic transfer function of digital programmable low pass filter
K_{active}	active stiffness of feedback control system.
P	probe distribution matrix.
$x^*(s)$	rotor motion at probe location.
$x_{in}^*(s)$	hydraulic actuator input displacement, or piezoelectric actuator tip displacement.
$W_i(t')$	state space variables of feedback electromechanical component (i=1,...,7).
ξ	sensitivity of the probes (7874 V/m).

INTRODUCTION

AVC has been applied to various rotorbearing systems for suppressing vibration by adding active damping or shifting critical speeds. An AVC system consists of sensors, controller (analog or digital), power amplifiers, and actuators. Although considerable research has been done on developing effective active control algorithms,

Presented at the International Gas Turbine and Aeroengine Congress and Exposition
The Hague, Netherlands — June 13–16, 1994
This paper has been accepted for publication in the Transactions of the ASME
Discussion of it will be accepted at ASME Headquarters until September 30, 1994

optimal control strategies, robust control, and QFT, much less has been done on actuator development. Piezoelectric actuators, magnetic bearing, and electromagnetic shakers are used as actuators due to their high bandwidth, large stroke, and force. Desirable features for actuators with AVC application on rotating machinery such as jet and rocket engine includes: small size for compactness, high force and stroke, and high/low temperature operation. A closed loop electromechanical simulation model also is essential for designing rotorbearing system AVC. Accurate predictions of forced response, critical speeds and stability are required to assure machinery health and reliability.

The previous test results of the current authors showed unbalance, subsynchronus and transient suppression by incorporating a PD controller and piezoelectric actuator (Palazzolo, et.al., 1991). Subsequent papers by the authors examined electromechanical stability simulation for the piezo-actuator AVC system (Lin, et.al, 1991) and automated feedback gain selection (Palazzolo, et.al., 1991) for the piezo-actuator AVC system. Piezo stacks may be too large or environmentally susceptible to locate in the volume envelope adjacent to an aircraft engine bearing. Hence, the concept of a hydraulic actuator, remotely driven by a piezoelectric stack was conceived. The output piston and transmission tube would be sufficiently small to position in the bearing compactment. Rashidi and DiRusso (1991) and also Ulbrich (1991) conducted research on a hydraulic actuator system for AVC. These research efforts employed a membrane construction for the piston which would provide a permanent seal. This configuration could be prone to accumulate bubbles reducing the effectiveness of the actuator, may fail from high cycle fatigue, or may reduce output stroke due to secondary deformation in the membrane. In addition, wear limitations, large space requirements, and low frequency response of mechanical valves limit the engineering application. Montague, et.al (1991) detected leakage and fatigue problems in their membrane type hydraulic actuator experiments. Tang, Palazzolo, et.al (1993) developed a new piezohydraulic actuator system for rotorbearing AVC. The configuration consists of a piezoelectric actuator and hydraulic transmission line with a liquid plastic fluid. AVC tests on an air turbine driven-dual overhung rotating test rig verified the effectiveness of this new actuator system for different stainless tube lengths and diameters.

A closed loop simulation of the AVC dynamic system is required to predict the system's stability, critical speeds, and unbalance response. Lin and Palazzolo (1991) used a 2nd order low pass electric filter to model the component's frequency characteristics. Maslen and Bielk (1991) presented an approach for coupling the frequency dependent components of the feedback loop to a structural finite element model with generic defined transfer functions. However, no details were provided for curve fitting, state space variable transformation, and electromechanical system coupling procedure. Ku and Chen (1992) presented a F.E. based method for stability analysis of electromechanical system (ES) model for an industry pump. Ramesh and Kirk (1992) made a comparison of closed loop simulation between the F.E. approach and transfer matrix method. Tang and Palazzolo (1993a) presented a general methodology which couples a finite element based model of the rotor with state space models of feedback control electromechanical components. This method was first applied to a cryogenic magnetic bearing test rig at NASA Lewis to predict the stability boundary and critical speeds with various feedback controllers. Good agreement was achieved between test and simulation.

This paper presents the active vibration control results of an air turbine driven test rig at NASA Lewis with a piezohydraulic actuator system. The closed loop electromechanical simulation method which accounts for non-ideal behavior of the feedback components is employed in predicting the unbalance response with and without active vibration control. Figure 1a shows the air turbine test rig assembly, and Figure 1b shows the piezohydraulic actuator system. The hybrid piezohydraulic actuator consists of a piezoelectric tube and output piston/cylinder, as shown in figure 2. The piezo stack is rated for a 90 micron stroke, 3000. N maximum force and 3. khz resonance. The transmission fluid is a specially developed liquid plastic (Tang, 1993 b) and is sealed at the pistons with double "O" rings. The tubes are vacuum filled to prevent bubble formation in the fluid.

TEST RIG AND SYSTEM MODEL

A sketch of a doubly overhung, air turbine driven test rig, and a diagram of the AVC feedback electromechanical components is shown in figure 3. This test rig includes a 2.5 cm diameter shaft which is 61.0 cm in length, a 14.0 N overhung disc which is 13.0 cm in diameter and two squirrel cage mounted ball bearings. The closed loop AVC system consists of a hybrid piezo-hydraulic actuator system which is integrated in a block with x and y path copper tube transmission lines of OD 9.53 mm (3/8''), a hybrid PID controller which is composed of PID analog electric circuits, summer&buckout circuits, a digitally programmable low pass filter, signal amplifier, ATE power supply & BOP power amplifier. The outboard squirrel cage bearing which has stiffness 1.4E+6 N/m is externally forced by the x and y pair of piezohydraulic actuators. The inboard squirrel cage bearing is in passive contact with an orthogonal pair of piezoelectric actuators which are turned off electrically and have a stiffness of 6.6E+6 N/m in each direction. Figure 4 shows the rotorbearing finite element model and control flow diagram for the system shown in figure 3. The rotor was modeled by beam elements with gyroscopics. The feedback electromechanical components are represented with independent state space equation matrices.

TRANSFER FUNCTION REPRESENTATIONS OF THE CLOSED LOOP ELECTROMECHANICAL MODEL

The general equation of an n degree of freedom model for the rotorbearing system may be expressed as;

$$\begin{bmatrix} I & 0 \\ 0 & I \end{bmatrix}_{2n\times 2n}\begin{Bmatrix} \dot{X}(t) \\ \ddot{X}(t) \end{Bmatrix}_{2n\times 1}+\begin{bmatrix} M^{-1}C & M^{-1}K \\ -I & 0 \end{bmatrix}_{2n\times 2n}\begin{Bmatrix} \dot{X}(t) \\ X(t) \end{Bmatrix}_{2n\times 1}=\begin{Bmatrix} M^{-1}F_u(t) \\ 0 \end{Bmatrix}_{2n\times 1}+\begin{Bmatrix} M^{-1}F_c(t) \\ 0 \end{Bmatrix}_{2n\times 1} \tag{1}$$

where

$F_u(t)$ unbalance force vector or external force vector (n×1)

$F_c(t)$ control force vector (n ×1)

M mass matrix (n ×n)

C damping coefficient matrix (n ×n)

K stiffness coefficient matrix (n ×n)

$X(t)$ displacement vector (n ×1)

$\dot{X}(t)$ velocity vector (n ×1)

$\ddot{X}(t)$ acceleration vector (n ×1)

n number of degrees of freedom for a rotorbearing system dynamic model

where I represents the identify matrix. Equation (1) may he time scaled to reduce the possibility of numerical problems which may occur in the closed loop dynamic analysis.

Set;

$$t'=\Delta t \quad and \quad dt=\frac{1}{\Delta}dt' \tag{2}$$

where

Δ represents a time scale factor (usually between 10E+3 and 10E+6)

Substitute equation (2) into equation (1) to obtain the final form;

$$\begin{bmatrix} I & 0 \\ 0 & I \end{bmatrix}\begin{Bmatrix} \dot{X}(t') \\ \ddot{X}(t') \end{Bmatrix}+\begin{bmatrix} \frac{M^{-1}C}{\Delta} & \frac{M^{-1}K}{\Delta^2} \\ -I & 0 \end{bmatrix}\begin{Bmatrix} \dot{X}(t') \\ X(t') \end{Bmatrix}=\begin{Bmatrix} \frac{M^{-1}}{\Delta^2}F_u(t') \\ 0 \end{Bmatrix}+\begin{Bmatrix} \frac{M^{-1}}{\Delta^2}F_c(t') \\ 0 \end{Bmatrix} \tag{3}$$

The dynamic characteristics of the feedback electromechanical components can be represented in transfer function forms. These forms are ohtained hy curve fitting experimental data to complex rational functions. This approach. may yield open-loop unstable representation of the individual components, indicated hy both positive and negative coefficients in the transfer function's denominator. This results from the imperfect representation of the component and may he eliminated by deleting all negative coefficient higher order terms in the denominator. These deleted terms are very small and are thus neglected. This was performed in all cases discussed below, and resulted in no detectable change in the goodness of the curve fit. It should also be recognized that open loop instability of an individual component in the feedback loop does not necessarily produce total system instability since other sources of phase lead (damping) may exist in the system.

The PID hybrid controller consists of three main parts: PID analog circuits, summer & buckout circuit, and

digital programmable low pass filter. In figure 4, $G_1(s)$ represents the transfer function of the hybrid controller derivative path from the rotor displacement x*(s) to the derivative output V_2. Hence;

$$G_1(s,G_C)=\frac{V_2(s)}{x^*(s)}=1.414\xi G_C G_d^*(s)$$
$$=\frac{1.414\xi G_C 3.97E-5s}{1+3.21E-5s+3.78E-10s^2+2.2AE-15s^3-1.48E-21s^4+7.47E-27s^5}$$
$$\approx\frac{1.414\xi G_C 3.97E-5s}{1+3.21E-5s+3.78E-10s^2+2.2AE-15s^3} \quad (4)$$

ξ is the sensitivity of the displacement probes (7874 V/m). The term 1.414ξ is the equivalent sensitivity of the probes due to their 45^0 mounting.

$x^*(s)$ is rotor displacement of the node which the probe senses

G_C is the adjustable derivative path gain of the hybrid controller

$G_d^*(s)$ is a unit transfer function of the input signal V_1 to output V_2 in figure 4, when G_K=0, and G_C=1.0. The term $G_d^*(s)$ was measured by spectrum analysis, and has the curve fit shown in figure 5. The term $G_2(s)$ is the transfer function of the hybrid controller proportional path from displacement x*(s) to hybrid controller output V_3.

$$G_2(s,G_K)=\frac{V_3(s)}{x^*(s)}=1.414\xi G_K G_p^*(s)$$
$$=\frac{1.414\xi G_K 0.92}{1+1.69E-5s+6.39E-11s^2+2.04E-16s^3-8.25E-23s^4-2.05E-27s^5}$$
$$\approx\frac{1.414\xi G_K 0.92}{1+1.69E-5s+6.39E-11s^2+2.04E-16s^3} \quad (5)$$

and G_K is the adjustahle proportional gain.

The term $G_p^*(s)$ is the unit transfer function of the input V_1 to output V_3 in figure 4, when G_K=1.0, and G_C=0. Figure 6 shows the curve fit for $G_p^*(s)$. The summer & buckout circuits in the controller have frequency dependent characteristics at the higher frequency ranges. Their transfer function $G_3(s)$ is given by a curve fit to the measured transfer function as shown in figure 7. The term $G_4(s, f_c)$ represents the transfer function of the digitally programmable low pass filter which has a cut-off frequency f_c.

$$G_3(s)=0.\frac{92}{1+1.42E-5s+4.77E-11s^2} \quad (6)$$

$$G_4(s,f_c)=\frac{K_0}{1+b_1s+b_2s^2+\cdots+b_ns^n} \quad (7)$$

The complete transfer function of the hybrid controller is a combination of equations (4),(5),(6), and (7), which gives;

$$G_{HC}(s)=[G_1(s,G_C)+G_2(s,G_K)]G_3(s)G_4(s,f_c) \quad (8)$$

where;

$G_{HC}(s)$ hybrid controller transfer function

The correlation of results obtained using equation (8) and test results at a combination of gains G_C=10.0 db, and G_K=3 db is shown in figure 9. The transfer function $G_5(s)$ which represents the dynamic model of the piezoelectric actuator in figure 4 is given by (Tang, 1993);

$$G_5(s)=\frac{5.2E-7+2.8E-17s^2}{1+8.843E-16s+1.784E-9s^2+4.35E-16s^3+8.26E-20s^4} \quad (9)$$

The last component in the feedhack path is the hydraulic actuator. Its output force characteristic was described in (Tang, 1993) as;

$$F_{out}(s)=G_6(s)\,(x_{in}^*(s)-G_7(s)x^*(s)) \quad (10)$$

where

$$G_6(s)=\frac{1.36\ 10^6+8.726s}{1+1.285\ 10^{-4}s-1.2638\ 10^{-8}s^2}\approx\frac{1.36\ 10^6+8.726s}{1+1.285\ 10^{-4}s} \quad (11)$$

$$G_7(s)=-\frac{0.42+1.189\ 10^{-3}s}{1+1.0411\ 10^{-3}s-4.861\ 10^{-7}s^2}\approx-\frac{0.42+1.189\ 10^{-3}s}{1+1.0411\ 10^{-3}s} \quad (12)$$

$x_{in}^*(s)$ hydraulic actuator input piston displacement, or piezoelectric actuator tip displacement.

$F_{out}(s)$ the control force acting on the outboard bearing case through the hydraulic actuator output piston.

The terms $G_6(s)$ and $G_7(s)$ were measured in bench tests of the actuator.

STATE SPACE REPRESENTATION OF THE FEEDBACK ELECTROMECHANICAL MODEL

The standard state space representation of transfer functions of any feedback component can be obtained by the transform method (Tang, Palazzolo, et.al, 1993). Hence, the transfer function $G_1(s,G_C)$ of the hybrid controller derivative path in equation (4) can be written in state space equation form as;

$$\begin{aligned} \dot{W}_1(t') &= A_1 W_1(t') + B_1 x^*(t') \\ V_2(t') &= C_1 W_1(t') \end{aligned} \tag{13}$$

where $W_1(t')$ is a 5×1 state variable vector, and

$$A_1 = \begin{pmatrix} 0 & 1 & 0 & 0 & 0 \\ 0 & 0 & 1 & 0 & 0 \\ & & & & \ddots \\ 0 & 0 & 0 & 0 & 1 \\ -\frac{1}{\Delta^5 b_5} & -\frac{b_1}{\Delta^4 b_5} & -\frac{b_2}{\Delta^3 b_5} & -\frac{b_3}{\Delta^2 b_5} & -\frac{b_4}{\Delta b_5} \end{pmatrix}, \quad B_1 = \begin{pmatrix} 0 \\ 0 \\ \vdots \\ 0 \\ \frac{1}{\Delta^5 b_5} \end{pmatrix} \tag{14}$$

$$C_1 = (0 \quad 1.414\xi G_c a_1 \Delta \quad 0 \quad 0 \quad 0) \tag{15}$$

$$\begin{aligned} a_0 &= 0, \ a_1 = -3.9E\text{-}5, \ b_1 = 3.21E\text{-}5, \ b_2 = 3.78E\text{-}10 \\ b_3 &= 2.24E\text{-}15, \ b_4 = -1.48E\text{-}21, \ b_5 = -7.47E\text{-}27 \end{aligned} \tag{16}$$

State space representations of the remaining components are listed below;

Hybrid Controller Proportional Path

$$\begin{aligned} \dot{W}_2(t') &= A_2 W_2(t') + B_2 x^*(t') \\ V_3(t') &= C_1 W_2(t') \end{aligned} \tag{17}$$

$$A_2 = \begin{pmatrix} 0 & 1 & 0 & 0 & 0 \\ 0 & 0 & 1 & 0 & 0 \\ & & & & \ddots \\ 0 & 0 & 0 & 0 & 1 \\ -\frac{1}{\Delta^5 b_5} & -\frac{b_1}{\Delta^4 b_5} & -\frac{b_2}{\Delta^3 b_5} & -\frac{b_3}{\Delta^2 b_5} & -\frac{b_4}{\Delta b_5} \end{pmatrix}, \quad B_2 = \begin{pmatrix} 0 \\ 0 \\ \vdots \\ 0 \\ \frac{1}{\Delta^5 b_5} \end{pmatrix} \tag{18}$$

$$C_2 = (1.414\xi G_c a_0 \quad 0 \quad 0 \quad 0 \quad 0 \quad 0) \tag{19}$$

$$\begin{aligned} a_0 &= 0.92, \ a_1 = 0, \ b_1 = 1.69E\text{-}5, \ b_2 = 6.39E\text{-}11 \\ b_3 &= 2.04E\text{-}16, \ b_4 = -8.25E\text{-}23, \ b_5 = -2.05E\text{-}27 \end{aligned} \tag{20}$$

Summer and DC Bias Buckout

$$\begin{aligned} \dot{W}_3(t') &= A_3 W_3(t') + B_3 (V_2(t') + V_3(t')) \\ &= A_3 W_3(t') + B_{31} W_1(t') + B_{32} W_2(t') \\ V_4(t') &= C_3 W_3(t') \end{aligned} \tag{21}$$

$$A_3 = \begin{pmatrix} 0 & 1 \\ -\frac{1}{\Delta^2 b_2} & -\frac{b_1}{\Delta b_2} \end{pmatrix}$$

$$B_{31} = B_3 C_2 = 1.414\xi G_C a_1 \begin{pmatrix} 0 & 0 & 0 & 0 & 0 & 0 \\ 0 & \frac{1}{\Delta b_2} & 0 & 0 & 0 & 0 \end{pmatrix} \tag{22}$$

$$B_{32} = B_3 C_3 = 1.414\xi G_g a_0 \begin{pmatrix} 0 & 0 & 0 & 0 & 0 & 0 \\ \frac{1}{\Delta^2 b_2} & 0 & 0 & 0 & 0 & 0 \end{pmatrix} \tag{23}$$

$$C_3 = (a_0 \quad 0) \tag{24}$$

$$a_0 = 0.92, \ a_1 = 0, \ b_1 = 1.42tE\text{-}5, \ b_2 = 4.775E\text{-}t1 \tag{25}$$

Low Pass Filter

$$\begin{aligned}\dot{W}_4(t') &= A_4W_4(t')+B_4V_4(t') \\ &= A_4W_4(t')+B_4C_3W_3(t') \\ V_5(t') &= C_4W_4(t')\end{aligned} \tag{26}$$

$$A_4=\begin{pmatrix} 0 & 1 & 0 & 0 \\ 0 & 0 & 1 & 0 \\ 0 & 0 & 0 & 1 \\ -\frac{1}{\Delta^4 b_4} & -\frac{b_1}{\Delta^3 b_4} & -\frac{b_2}{\Delta^2 b_4} & -\frac{b_3}{\Delta^1 b_4} \end{pmatrix}, \quad B_4=\begin{pmatrix} 0 \\ 0 \\ \vdots \\ \frac{1}{\Delta^4 b_4} \end{pmatrix} \tag{27}$$

$$C_4=(a_0 \quad 0 \quad 0 \quad 0) \tag{28}$$

$$a_0=0.87,\ b_1=\frac{3.95E-1}{f_c},\ b_2=\frac{8.262E-2}{f_c^2},\ b_3=\frac{9.97E-3}{f_c^3},\ b_4=\frac{5.74E-4}{f_c^4} \tag{29}$$

Piezoelectric Actuator

$$\begin{aligned}\dot{W}_5(t') &= A_5W_5(t')+B_5V_5(t') \\ &= A_5W_5(t')+B_5C_4W_4(t') \\ V_6(t') &= C_5W_5(t')\end{aligned} \tag{30}$$

$$A_5=\begin{pmatrix} 0 & 1 & 0 & 0 \\ 0 & 0 & 1 & 0 \\ 0 & 0 & 0 & 1 \\ -\frac{1}{\Delta^4 b_4} & -\frac{b_1}{\Delta^3 b_4} & -\frac{b_2}{\Delta^2 b_4} & -\frac{b_3}{\Delta^1 b_4} \end{pmatrix}, \quad B_5=\begin{pmatrix} 0 \\ 0 \\ \vdots \\ \frac{1}{\Delta^4 b_4} \end{pmatrix} \tag{31}$$

$$C_5=GPA(A_0\ a_1\ a_2\Delta^2) \text{ where } (G_{PA}=G_{preston}+G_{BOP+ATE}=15.0) \tag{32}$$

$$a_0=5.20E-8,\ a_1=0,\ a_2=2.8E-18 \tag{33}$$
$$b_1=1.0E-5,\ b_2=2.0E-5,\ b_3=8.0E-15,\ b_4=7.5E-19$$

and

$G_{preston}$ Preston Amplifier Gain =2.0, cut-off frequency 100K Hz

$G_{BOP+ATE}$ BOP Power Amplifier and ATE Power Supply Gain=7.5

Hydraulic Actuator

(I)

$$\begin{aligned}\dot{W}_7(t') &= A_7W_7(t') + B_7x^*(t') \\ V_8(t') &= C_7W_7(t')\end{aligned} \tag{34}$$

$$A_7=\begin{pmatrix} 0 & 1 \\ -\frac{1}{\Delta^2 b_2} & -\frac{b_1}{\Delta b_2} \end{pmatrix}, \quad B_7=\begin{pmatrix} 0 \\ \frac{1}{\Delta^2 b_2} \end{pmatrix} \tag{35}$$

$$C_7=(a_0 \quad a_1\Delta) \tag{36}$$

$$a_0=0.42,\ a_1=1.189E-3,\ b_1=1.041E-3,\ b_2=-4.86E-7 \tag{37}$$

(II)

$$\begin{aligned}\dot{W}_6(t') &= A_6W_6(t') + B_6C_5W_5(t') + B_6C_7W_7(t') \\ f_c^*(t') &= 2*C_6W_6(t')\end{aligned} \tag{38}$$

$$A_6=\begin{pmatrix} 0 & 1 \\ -\frac{1}{\Delta^2 b_2} & -\frac{b_1}{\Delta b_2} \end{pmatrix}, \quad B_6=\begin{pmatrix} 0 \\ \frac{1}{\Delta^2 b_2} \end{pmatrix} \tag{39}$$

$$C_6=(a_0 \quad a_1\Delta) \tag{40}$$

$$a_0=1.36E+6,\ a_1=8.726,\ b_1=1.286E-4,\ b_2=-1.264E-8 \tag{41}$$

The term $f_C^*(t')$ is the control force provided by the hydraulic actuator and is the state variable output of the state space equation (38).

ASSEMBLY OF THE CLOSED LOOP EQUATIONS

A complete closed loop dynamic simulation can be

implemented by the following 3 steps. Step 1 is to identify the transfer function representations of all feedback components which were curve fitted in the previous section. Step 2 is to transform the transfer function to state space representations. Step 3 is to rearrange the state space equations and define the control force distribution matrix and sensor distribution matrix which couple the feedback electromechanical representations with the rotorbearing dynamic model into a total system matrix.

The closed loop dynamic equation of the air turbine test rig with the AVC is obtained by combining state space equations (13), (17), (21), (26), (30), (34), (38). Equation (3) which represents the rotorbearing dynamic model can be rearranged by shifting the control force vector from the right side of the equation to the left side;

$$\begin{pmatrix} I & 0 \\ 0 & I \end{pmatrix} \begin{pmatrix} \dot{X}(t') \\ \ddot{X}(t') \end{pmatrix} + \begin{pmatrix} \frac{M^{-1}C}{\Delta} & \frac{M^{-1}K}{\Delta^2} \\ -I & 0 \end{pmatrix} \begin{pmatrix} \dot{X}(t') \\ X(t') \end{pmatrix} - \begin{pmatrix} \frac{M^{-1}}{\Delta^2} F_C(t') \\ 0 \end{pmatrix} = \begin{pmatrix} \frac{M^{-1}}{\Delta^3} F_U(t') \\ 0 \end{pmatrix} \tag{42}$$

Equation (13) represents the derivative path of the hybrid controller and can be rewritten as;

$$\dot{W}_1(t') - A_1 W_1(t') - B_1 x^*(t') = 0 \tag{43}$$

where $x^*(t')$ is the rotor displacement which the probe senses, and can be represented by;

$$x^*(t') = PX(t') \tag{44}$$

By substituting equation (44), equation (43) can also be written as;

$$\dot{W}_1(t') - A_1 W_1(t') - B_1 PX(t') = 0 \tag{45}$$

where P is defined as the probe distribution matrix. For a probe at the ith global dof number, the P matrix has the following form;

$$P = \begin{matrix} \\ i \text{ row} \end{matrix} \begin{matrix} \overset{i \text{ column}}{\overset{\downarrow}{\begin{pmatrix} 0 & 0 & \cdots & 0 & \cdots & 0 \\ \vdots & \vdots & \vdots & \vdots & \cdots & \vdots \\ 0 & \cdots & 1 & 0 & \cdots & 0 \\ \vdots & \vdots & \vdots & \vdots & \cdots & \vdots \\ 0 & 0 & \cdots & 0 & \cdots & 0 \end{pmatrix}}} \end{matrix} \tag{46}$$

By substituting equation (46), equation (17) which is the state space representation of the proportional path becomes;

$$\dot{W}_2(t') - A_2 W_2(t') - B_2 PX(t') = 0 \tag{47}$$

Similarly, equations (21), (26), (30), (34), and (38) can be rewritten as;

$$\dot{W}_3(t') - A_3 W_3(t') - B_{31} W_1(t') - B_{32} W_2(t') = 0 \tag{48}$$

$$\dot{W}_5(t') - A_5 W_5(t') - B_5 C_4 W_4(t') = 0 \tag{49}$$

$$\dot{W}_6(t') - A_6 W_6(t') - B_6 C_5 W_5(t') - B_6 C_7 W_7(t') = 0 \tag{50}$$

and

$$\dot{W}_7(t') - A_7 W_7(t') - B_7 x^*(t') = 0 \tag{51}$$

$$\dot{W}_7(t') - A_7 W_7(t') - B_7 PX(t') = 0 \tag{52}$$

For equation (38), the control force can be written as;

$$f_c^*(t') - 2 * C_6 W_6(t') = 0 \tag{53}$$

Define;

$$F_C(t') = \begin{pmatrix} 0 \\ \vdots \\ 1 \\ 0 \\ \vdots \end{pmatrix} f_c^*(t') = G f_c^*(t') = 2.0\, G\, C_6\, W_6 \tag{54}$$

where G is called the control force distribution matrix. If the actuator is located at global degree of freedom number j, G has the following form;

$$G = \begin{pmatrix} 0 \\ \vdots \\ 1 \\ 0 \\ \vdots \end{pmatrix} \begin{matrix} \\ \\ j\text{th row} \\ \\ \\ \end{matrix} \tag{55}$$

By combining equations (42), (45), (47), (48), (50), (51),

(52), and (53) , the closed loop system dynamic equations can be written into a state space representation as;

$$\dot{Z}+Q\,Z=F \tag{56}$$

where;

Q dynamic matrix of closed loop AVC system

Z state space variable vector of closed loop AVC system

F state space force vector of closed loop AVC system

$$Q=\begin{pmatrix} \frac{M^{-1}C}{\Delta} & \frac{M^{-1}K}{\Delta^2} & 0 & 0 & 0 & 0 & \frac{2M^{-1}GC_5}{\Delta^2} & 0 & 0 \\ -I & 0 & 0 & 0 & 0 & 0 & 0 & 0 & 0 \\ 0 & -B_1P & -A_1 & 0 & 0 & 0 & 0 & 0 & 0 \\ 0 & -B_2P & 0 & -A_2 & 0 & 0 & 0 & 0 & 0 \\ 0 & 0 & -B_{31} & -B_{32} & -A_3 & 0 & 0 & 0 & 0 \\ 0 & 0 & 0 & 0 & -B_4C_3 & -A_4 & 0 & 0 & 0 \\ 0 & 0 & 0 & 0 & 0 & -B_5C_4 & -A_5 & 0 & 0 \\ 0 & 0 & 0 & 0 & 0 & 0 & -B_6C_5 & -A_6 & -B_6C_6 \\ 0 & -B_7P & 0 & 0 & 0 & 0 & 0 & 0 & -A_7 \end{pmatrix} \quad F=\begin{pmatrix} \frac{M^{-1}F_0(t')}{\Delta^2} \\ 0 \\ 0 \\ 0 \\ 0 \\ 0 \\ 0 \\ 0 \\ 0 \end{pmatrix} \tag{57}$$

The unbalance force in equation (56) can be written as;

$$F_0(t')=m_e\omega^2C_e\begin{pmatrix}\sin\omega t' & (X\ direction)\\ \cos\omega t' & (y\ direction)\end{pmatrix} \tag{58}$$

The steady response of the state variable vector is;

$$Z=\underline{Z}\sin\omega t' \tag{59}$$

where

m_e ; unbalance mass

C_e ; eccentricity distance

ω ; frequency (rad/s)

$\underline{Z}$; the complex amplitude of the state space vector

The unbalance response of a system with AVC can be obtained by solving equatio (56). The stability analysis of a closed loop AVC system can be performed by letting;

$$F=0,\quad and\quad Z=\underline{Z}e^{\lambda t'} \tag{60}$$

and solving the following eigenvalue and eigenvector problem;

$$(\lambda I+Q)\,\underline{Z}=0 \tag{61}$$

where

λ is the eigenvalue

$\underline{Z}$ is the eigenvector

CORRELATION OF SIMULATION AND TEST RESULTS

Active vibration control was used on the air turbine test rig with the piezohydraulic actuator system shown in figures 1a, 1b, and 2 at NASA Lewis. The tests were performed to compare unbalance response with control and without control. Unbalance response test results were obtained by adding an imbalance to the outboard disk at a radius of 50.8 mm (2.0 in) and measuring the unbalance response at the outboard disk, outboard bearing, middle shaft, inboard bearing, and inboard disk. Figures 10, and 11 show the first and second modeshapes with the piezohydraulic actuator and feedback PD control at gains G_K=5.6, and G_C=-40.0. The first natural frequency in figure 11 is less than without control due to an active stiffness (controller proportional gain is 5.6) which shifted the first natural frequency down to about 90 hz.

Closed loop unbalance response simulation was obtained by solving equation (56) with various test parameters (unbalance mass, controller gains, and probe locations). Figures 12 and 13 show the correlation of simulation and test results for unbalance responses (an unbalance mass m_e=0.6 g on the outboard disk) in the X direction at the outboard bearing location, and outboard disk location, respectively. The passive tare damping employed to match the uncontrolled response were 150 and 50 N.S./m, and were applied at the outboard bearing location and inboard bearing location respectively. The derivative gain and proportional gain of the hybrid controller are -40, and 5.6, respectively. The feedback active damping and active stiffness can be calculated by multiplying the derivative path transfer functions at frequency=0 or s=0. Hence, from figure 4, the active damping can be written as;

$$C_{active}=1.414\left(\left(\frac{G_1(s)}{s}\right)G_3(s)G_4(s)G_5(s)G_6(s)\right)_{s=0} \tag{62}$$

and from equations (4), (6), (7), (9), and (11), equation (62) can be written as;

$$C_{active} = 1.414 \times 7874 \times 3.97E-5 \times |G_C| \times 0.92 \times 0.87 \times 15 \times 5.2E-7 \times 2 \times 1.36E+6 \quad N\,s/m \tag{63}$$

when G_C=-40.0, the active damping is:

$$C_{active} = 1.414 \times 7874 \times 3.97E-5 \times 40.0 \times 0.92 \times 0.87 \times 15 \times 5.2E-7 \times 2 \times 1.36E+6 = 300\ N\,s/m \tag{64}$$

Similarly, by multiplying the proportional path transfer functions, the active stiffness can by written as;

$$K_{active} = 1.414\,\xi\left(G_2(s)G_3(s)G_4(s)G_5(s)G_6(s)\right)_{s=0} \tag{65}$$

By applying equations (5), (6), (7), (9), (11), and G_K=5.6, the active stiffness is:

$$K_{active} = 1.414 \times 7874 \times 0.92 \times 5.6 \times 0.92 \times 0.87 \times 15 \times 5.2E-7 \times 2 \times 1.36E+6 = 0.974E+6\ N/m \tag{66}$$

Figure 14 shows the effectiveness of the AVC with increasing levels of imbalance. Figures 15, and 16 show the unbalance responses at the outboard bearing and outboard disk locations after removing a ring which weighs 8.04 N (1.8 lbs) from the outboard disk to raise the critical speeds. Significant reductions in vibration were again achieved by the hybrid actuator system.

SUMMARY AND CONCLUSIONS

A compact piezohydraulic actuator system using liquid plastic as a transmission fluid, and a copper tube as a transmission line was employed in AVC of an air turbine test rig. Significant reductions of vibration were achieved at the first critical speed. A closed loop unbalance response simulation with AVC was also developed in this research. The new dynamic models of the piezoelectric actuator, hydraulic actuator, and digital programmable low pass filter were included in the closed loop system modeling. Transfer functions were identified from measured data and state space representations were employed to account for the non-ideal behavior of the feedback electromechanical components. This simulation approach was verified by good agreement with test results.

ACKNOWLEDGEMENTS

The authors thank NASA Lewis and the U.S. Army at NASA Lewis for funding this research. Sincere appreciation is also extended to Mr. Daniel Manchala for his assistance in testing and data acquisition, and Dr. Wenduan Li (Texas A&M University, Chemical Engineering) and Renee Udell for their assistance in hydraulic actuator bench test.

REFERENCES

DiRusso, Eliseo and Brown, Gerald V., 1992, "Tests of a Cryogenic Magnetic Bearing with Permanent Magnet Bias", *proceedings of the Third International Symposium on Magnetic Bearings*, Alexandria, Virginia.

Ku, C.-p.R., and Chen, H. M., 1992, "An Efficient Method for Stability Analysis for Active Magnetic Bearing System", *Proceedings of the Third International Symposium on Magnetic Bearings*, Alexandria, Virginia, July, pp.133-142.

Lin, R.R., Palazzolo, A.B., Kascak, A.F., Montague, G.T., 1991, "Electromechanical Simulation and Testing of Actively Controlled Rotordynamic Systems with Piezoelectric Actuators,", *Presented at the International Gas Turbine Conference*, Orlando, Florida, June 3-6, accepted for publication in the Transactions of the ASME

Lin, R. R., 1990, "Active Vibration Control of Rotorbearing Systems Utilizing Piezoelectric Pushers", Dissertation, pp.49-50, Texas A&M University, Mechanical Engineering.

Maslen, E. H. and Bielk, J. R., "Implementing Magnetic Bearing in Discrete Flexible Structure Models", Submitted to Transaction ASME, *Journal of Dynamics and Controls*, 1991.

Montague, G., et.al, 1991, "Hydraulic Actuator for Active Vibration Control", Senior Project, Cleveland State Univ., Dept. of Mechanical Engineering, June.

Palazzolo, A.B., Lin, R.R., Alexander, R.M., Kascak, A.F., Montague, G, 1991, "Test and Theory for Piezoelelectric Actuator-Active Vibration Control of Rotating Machinery," *Journal of Vibrations and Acoustics*, April, Vol.113, pp.167-175.

Palazzolo, A.B., Jagannathan, S., Kascak, A.F., Montague, G.T., and Kiraly, L.J., 1991, "Hybrid Active

Vibration Control of Rotorbearing Systems Using Piezoelectric Actuators," ASME hook No.G0644E, *Journal of Vibration and Acoustics*. January, 1993.

Ramesh, K. and Kirk, R. G., 1992, "Subharmonic Resonance Stability Prediction for Turbomachinery with Active Magnetic Bearings", *Proceedings of the Third International Symposium on Magnetic Bearings,* Alexandria, Virginia, July, pp.113-122.

Rashidi, Majid, DiRusso Eliseo, 1991, " Design of a Hydraulic Actuator for Active Control of Rotating Machinery", *Presented at the International GAS Turbine and Aeroengine Congress and Exposition,* Orlando, FL June 3-6.

Tang, P., Palazzolo, A.B, et.al., 1993a, "An Electromechanical Simulation Method for Active Vibration Control of a Magnetic Bearing Supported Rotor", *Presented at the International Gas Turbine and Aeroengine Congress and Exposition,* Cincinnati, Ohio, May 24-27, 93-GT-386.

Tang P., Palazzolo, A.B. et. al., 1993b, " Combined Piezoelectric-Hydraulic Actuator Based Active Vibration Control for Rotordynamic System", *presented to the 14th Biennial Conference on Mechanical Vibration and Noise,* Albuquerque, September 19-22. DE-Vol.62.

Tang P., 1993, "A Combined Piezoelectric-Hydraulic Actuator System and an Electromechanical Simulation Method for Active Vibration Control of Rotordynamic Systems", Dissertation, Texas A&M University, Mechanical Engineering, September. pp. 90-109.

Ulbrich, Heinz, Althaus Josef, 1992, "Active Bearing for Rotating Machinery", *Presented at Fourth International Symposium on Transport Phenomena and Dynamics of Rotating Machinery (ISROMAC-4),* Hawaii, April 5-8.

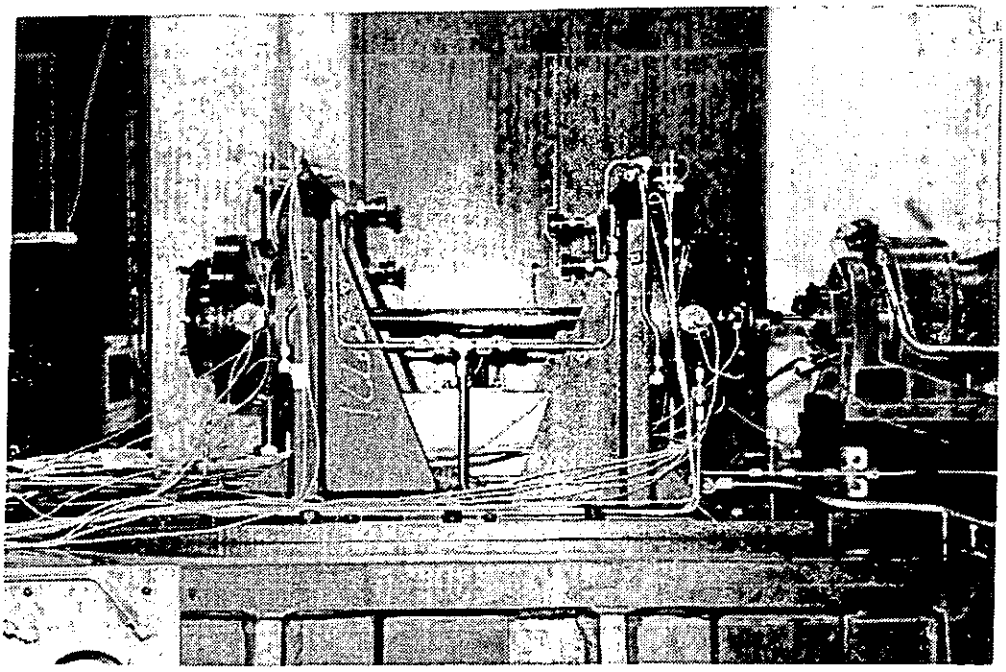

Figure 1a AVC Setup on the Gas Turbine Test Rig at NASA Lewis with Piezohydraulic Actuator System

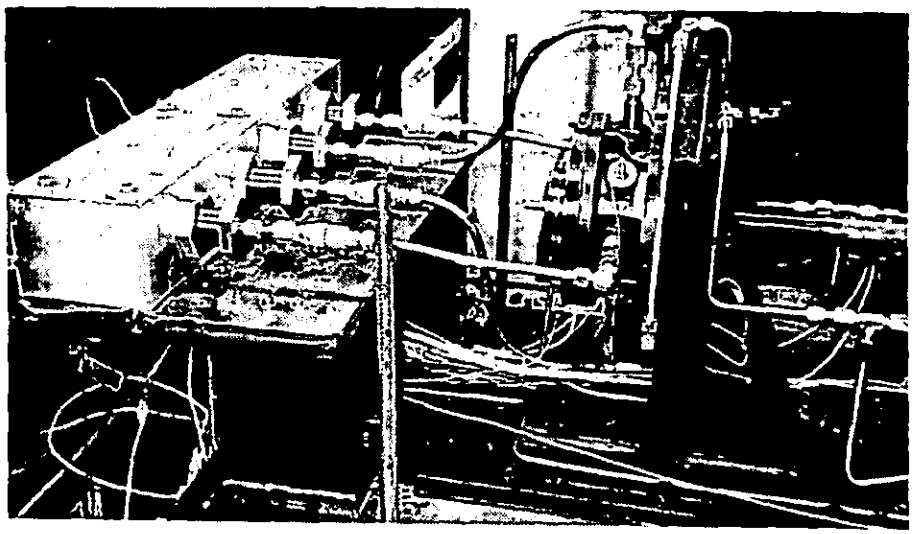

Figure 1b Piezohydraulic Actuator Setup on the Air turbine Test Rig at NASA Lewis

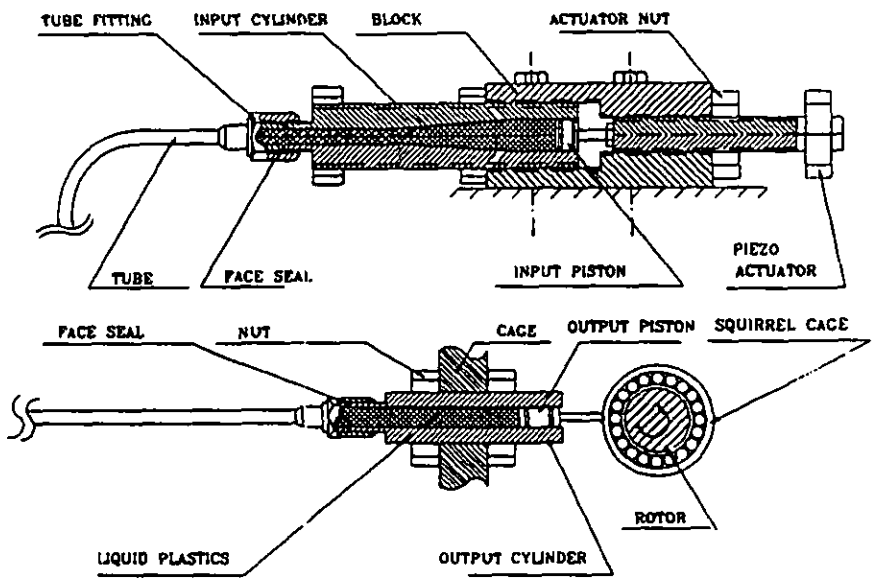

Figure 2 Combined Piezoelectric-Hydraulic Actuator System

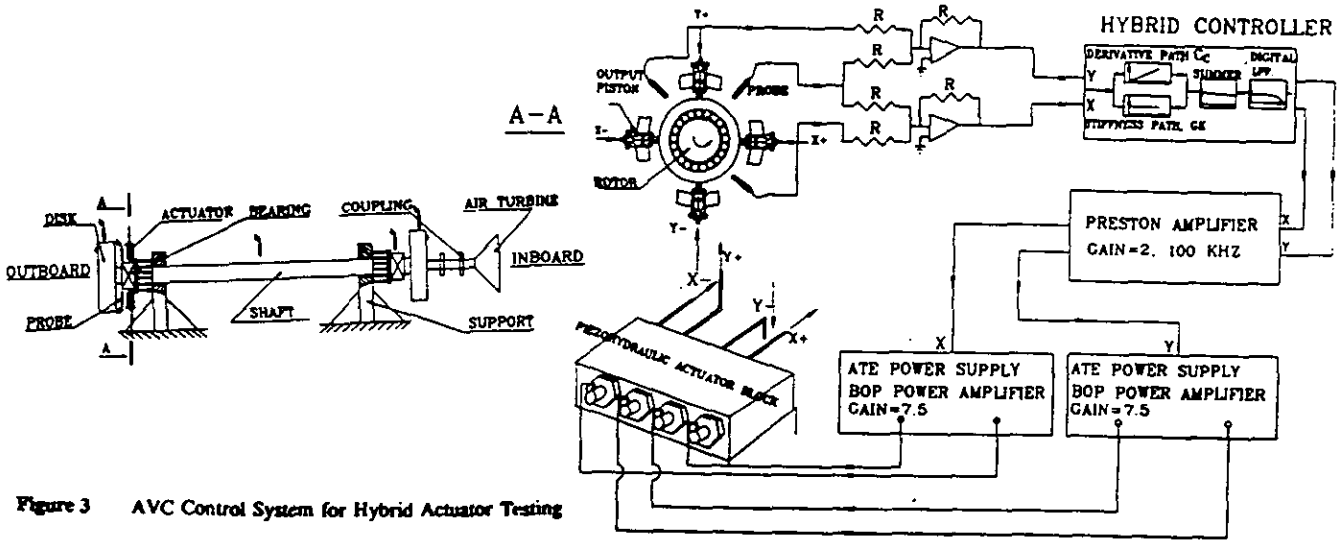

Figure 3 AVC Control System for Hybrid Actuator Testing

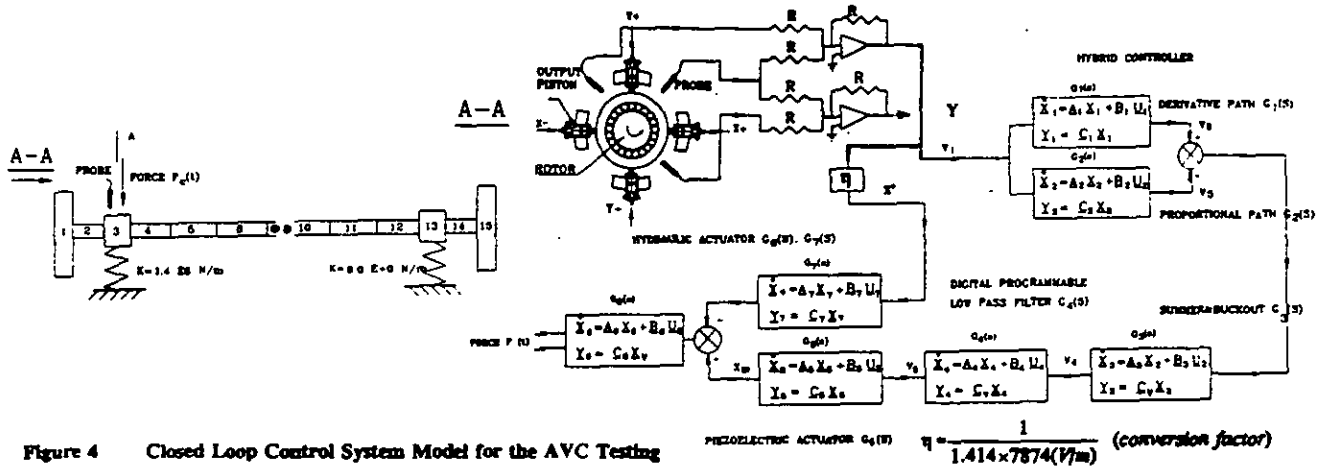

Figure 4 Closed Loop Control System Model for the AVC Testing

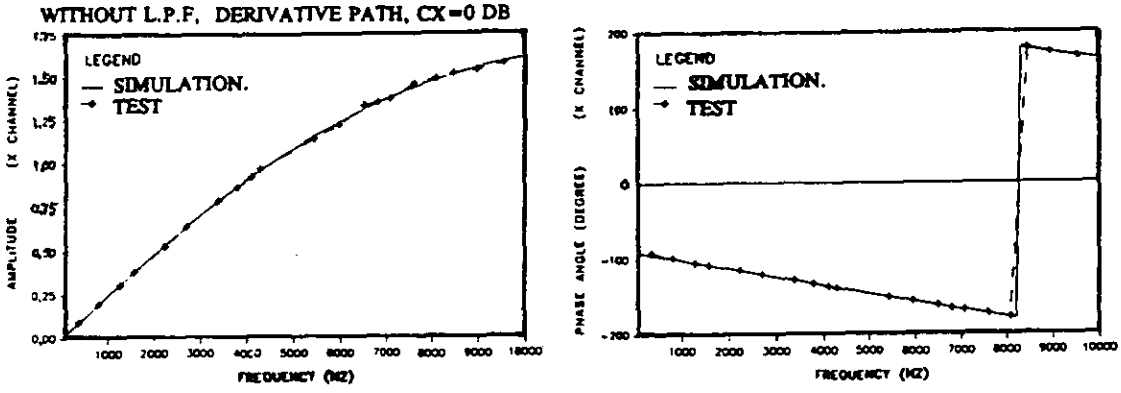

Figure 5 Curve Fit for Normalized Transfer Function $G_d^*(s)$ of the Controller Derivative Path

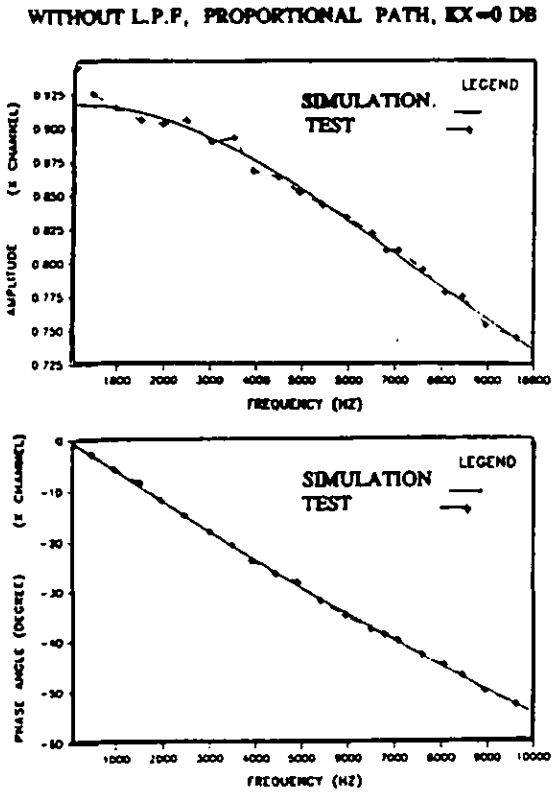

Figure 6 Curve Fit for Normalized Transfer Function $G_p{}^n(s)$

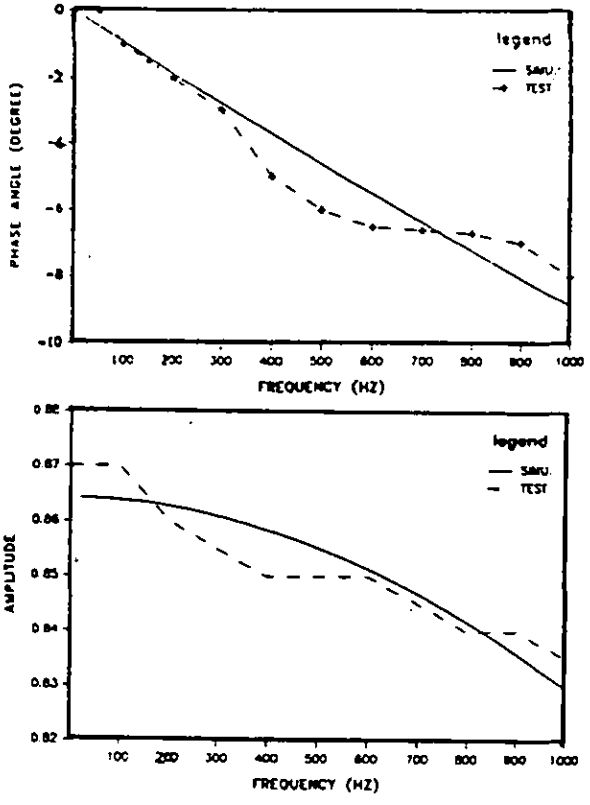

Figure 7 Curve Fit for Summer and Buckout Electric Circuit $G_3(s)$

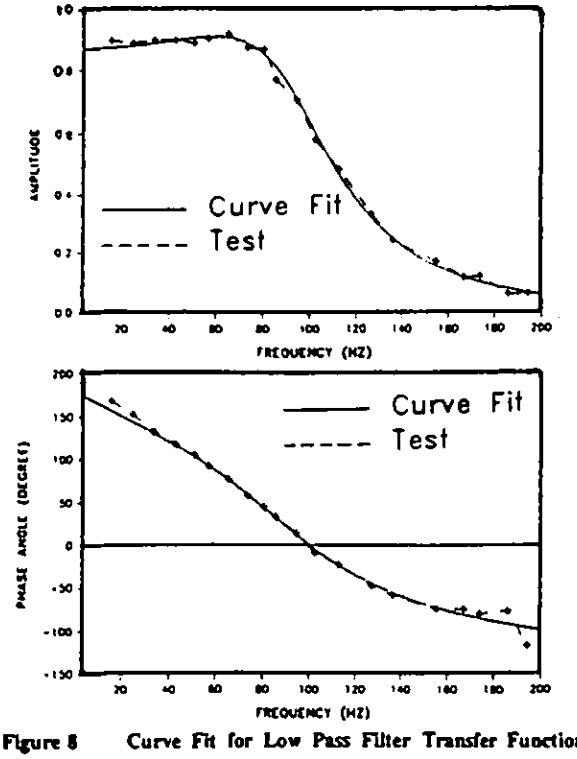

Figure 8 Curve Fit for Low Pass Filter Transfer Function

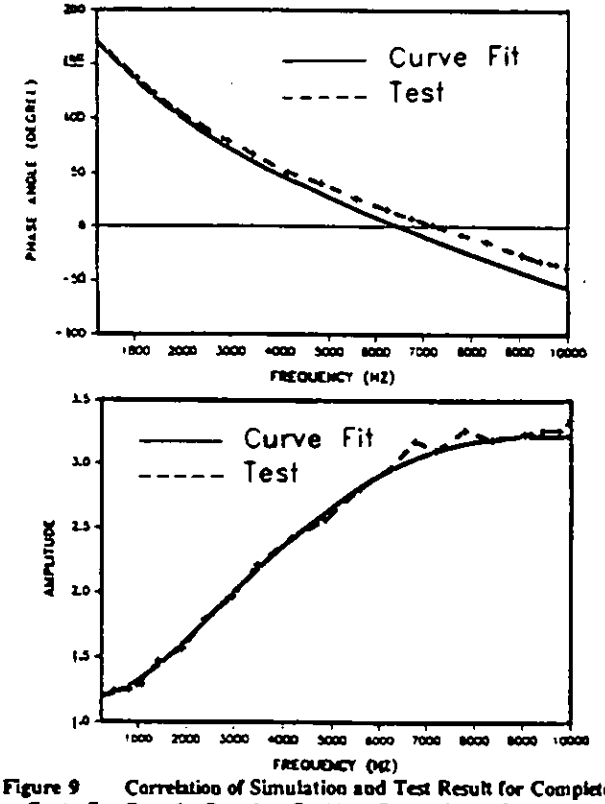

Figure 9 Correlation of Simulation and Test Result for Complete Controller Transfer Function $G_{BC}(s)$ at G_c=10.0 db, G_g=3.0 db

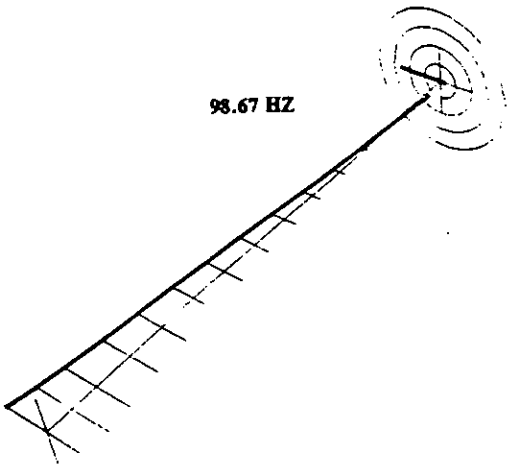

Figure 10 First Mode Shape of the Air Turbine with Piezohydraulic Actuator System AVC (Gains G_z=5.6, G_c=40.0) (98.67 HZ)

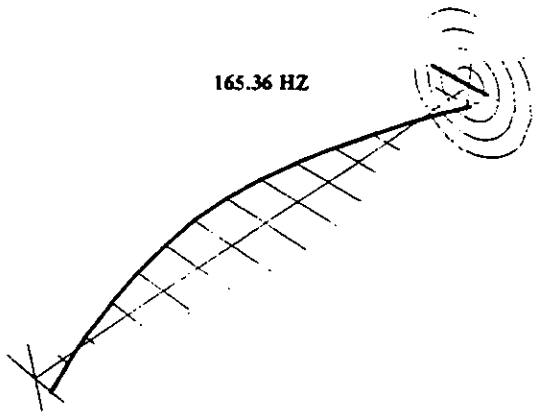

Figure 11 Second Mode Shape of the Air Turbine with Piezohydraulic Actuator System AVC (Gains G_z=5.6, G_c=40.0) (165.36 HZ)

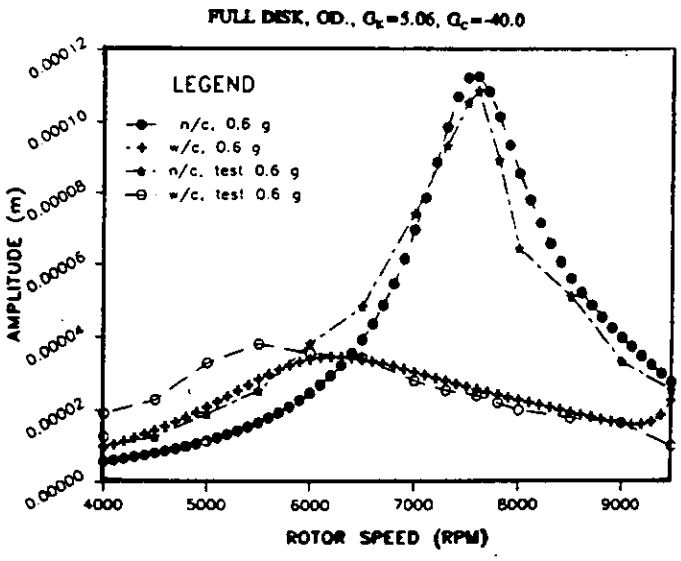

Outboard Bearing Damping =150 N/m/s

Inboard Bearing Damping =50 N/m/s

Figure 12 The Simulation and Test Unbalance Responses at Outboard Disk Location with/without AVC

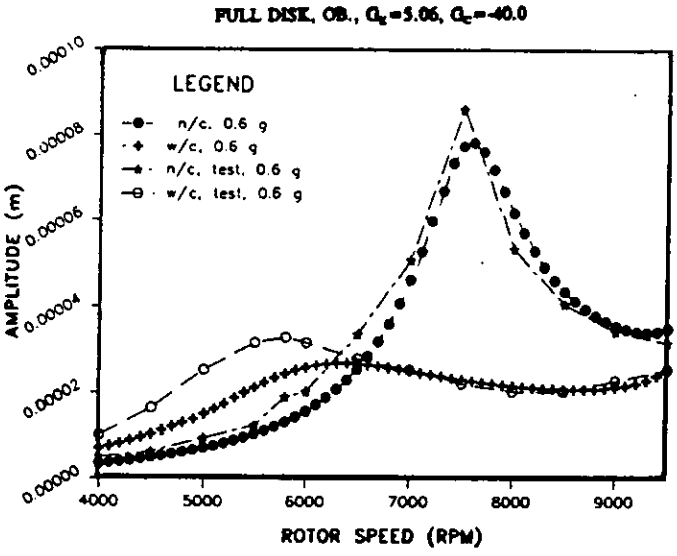

Figure 13 The Simulation and Test Unbalance Responses at Outboard Bearing Location with/without AVC

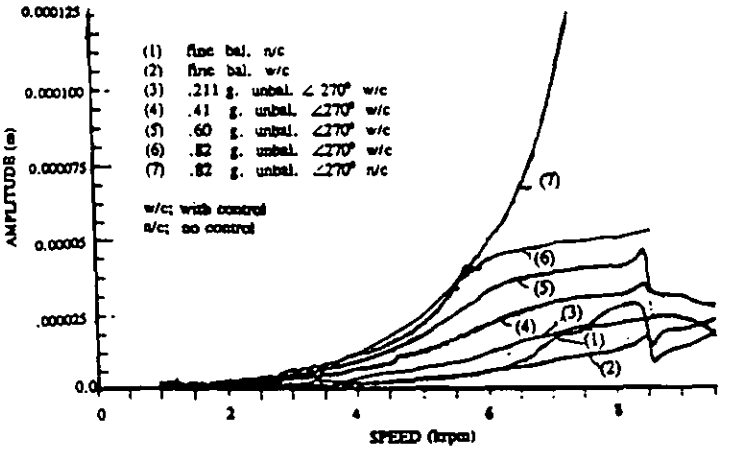

Figure 14 Test Imbalance Responses with Various Imbalance Masses at Outboard Disk Location in y direction with/without AVC

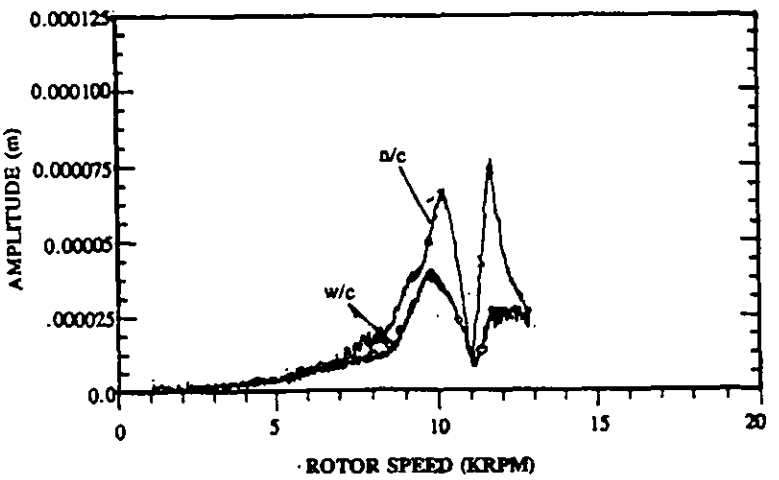

Figure 15 Test Unbalance Responses of Outboard Bearing Location with/without AVC with Outboard Ring Removed

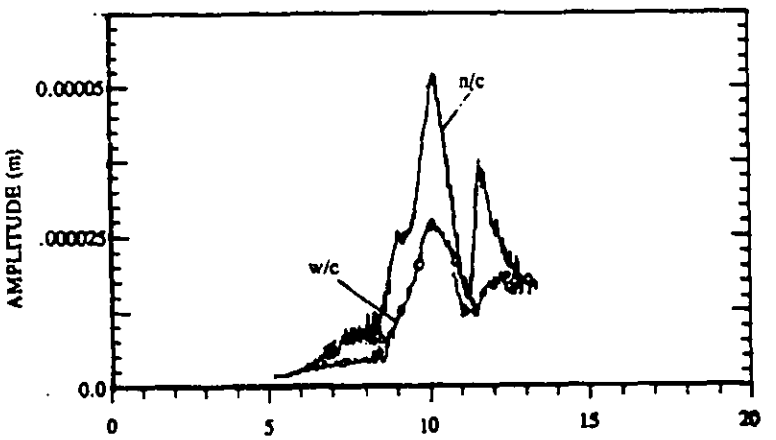

Figure 16 Test Unbalance Responses of Outboard Disk Location with/without AVC with the Outboard Ring Removed